Title

Phase-contrast MRI with hybrid one and two-sided flow-encoding and velocity spectrum separation

Journal

Magnetic Resonance in Medicine, 78(1)

ISSN

0740-3194

Authors

Wang, Da
Shao, Jiaxin
Ennis, Daniel B
et al.

Publication Date

2017-07-01

DOI

10.1002/mrm.26366

Peer reviewed

FULL PAPER

Magnetic Resonance in Medicine 00:00–00 (2016)

Phase-Contrast MRI with Hybrid One and Two-Sided Flow-Encoding and Velocity Spectrum Separation

Da Wang,[1,2] Jiaxin Shao,[1] Daniel B. Ennis,[1,2,3] and Peng Hu[1,2]*

Purpose: To develop and evaluate a phase-contrast MRI (PC-MRI) technique with hybrid one and two-sided flow-encoding and velocity spectrum separation (HOTSPA) for accelerated blood flow and velocity measurement.

Methods: In the HOTSPA technique, the two-sided flow encoding (FE) is used for two FE directions and one-sided is used for the remaining FE direction. Such a temporal modulation of the FE strategy allows for separations of the Fourier velocity spectrum into components for the flow-compensated and the three-directional velocity waveforms, accelerating PC-MRI by encoding three-directional velocities using only two repetition times (TRs) instead of four TRs as in standard PC-MRI. The HOTSPA was evaluated and compared with standard PC-MRI in the common carotid arteries of six healthy volunteers.

Results: Total volumetric flow and peak velocity measurements based on HOTSPA and the conventional PC-MRI were in good agreement with a bias of −0.005 mL (−0.1% relative bias error) for total volumetric flow and 1.21 cm/s (1.1% relative bias error) for peak velocity, although the total acquisition time was 50% of the conventional PC-MRI.

Conclusion: The proposed HOTSPA technique achieved nearly two-fold acceleration of PC-MRI while maintaining accuracy for total volumetric flow and peak velocity quantification by separating the paired acquisitions in the Fourier velocity spectrum domain. **Magn Reson Med 000:000–000, 2016. © 2016 International Society for Magnetic Resonance in Medicine**

Key words: phase contrast MRI; 4D-flow; temporal modulation

INTRODUCTION

Phase-contrast MRI (PC-MRI) has been used extensively for quantification of blood flow and velocity. In conventional PC-MRI, the flow-compensated (FC) and flow-encoded (FE) data are acquired in an interleaved fashion, and the blood flow velocity is encoded in the phase difference between the FC and FE data. Although PC-MRI is typically performed with FE gradients applied in the through-plane direction using two-dimensional (2D) acquisitions (1), the FE gradients can also be applied in more than one orientation, as in 2D tissue phase mapping (2,3) or four-dimensional (4D) flow PC-MRI (4). This permits capturing the blood flow or tissue motion along the slice, phase, and frequency encoding directions. For 4D-flow, however, the temporal sampling period (i.e., the time between two successive cardiac phases) is typically poorer (i.e., longer) than conventional 2D PC-MRI because of the need to acquire the FC data and three-directional (3D) FE data interleaved within each cardiac k-space segment. A long temporal sampling period and temporal footprint (i.e., the time span of the data used to reconstruct a single temporal phase) for PC-MRI underestimate peak velocity (5,6), which is an important index for diagnosis of carotid artery stenosis (7,8) and pressure gradients across valves (9). Temporal sampling period can be improved by reducing the views per segment (VPS, i.e., the number of k-space lines acquired for each cardiac phase per cardiac cycle), but this concomitantly increases the total image acquisition duration (10).

Fast MRI techniques such as non-Cartesian sampling (11,12), parallel imaging (13–16), k-t space acceleration (17,18), compressed sensing (19–21), and optimized gradient waveforms (22) have been developed to effectively reduce the total acquisition time of PC-MRI or to improve the temporal sampling period. The temporal sampling period may also be improved by several other techniques. A recently proposed shared velocity encoding (SVE) technique (5) uses interleaved two-sided velocity encodings and sliding window subtractions, which effectively shortens the temporal sampling period. However, the temporal footprint of each SVE cardiac phase is the same as traditional 2D PC-MRI. Furthermore, the implementation of the SVE technique for 4D-flow increases the temporal footprint (=6*TR*VPS) compared with conventional 4D-flow (=4*TR*VPS). The issue of temporal footprint is mitigated by the flow compensation view sharing (FCVS) technique (6), in which the FC data are undersampled and view-shared based on the assumption that the FC background phase data do not temporally change as fast as the FE data.

In this work, we propose a PC-MRI strategy with hybrid one and two-sided flow encoding and velocity spectrum separation (HOTSPA). The HOTSPA technique consists of three components: 1) the velocity encoding gradient polarity, which alternates between successive cardiac phases for two of the FE directions (i.e., two-sided flow encoding); 2) the velocity encoding gradient polarity, which remains one-sided along the remaining FE direction; and 3) the FC data, which are not explicitly

[1]Department of Radiological Sciences, David Geffen School of Medicine, University of California, Los Angeles, CA, USA.

[2]Biomedical Physics Interdepartmental Graduate Program, University of California, Los Angeles, CA, USA.

[3]Department of Bioengineering, University of California, Los Angeles, CA, USA.

*Correspondence to: Peng Hu, PhD, Department of Radiological Sciences, 300 UCLA Medical Plaza Suite B119, Los Angeles, CA 90095. E-mail: penghu@mednet.ucla.edu.

Grant support: Research reported in this publication was supported by the National Heart, Lung, and Blood Institute of the National Institutes of Health under Award Number R01HL127153.

Received 1 March 2016; revised 8 July 2016; accepted 9 July 2016

DOI 10.1002/mrm.26366

Published online 00 Month 2016 in Wiley Online Library (wileyonlinelibrary.com).

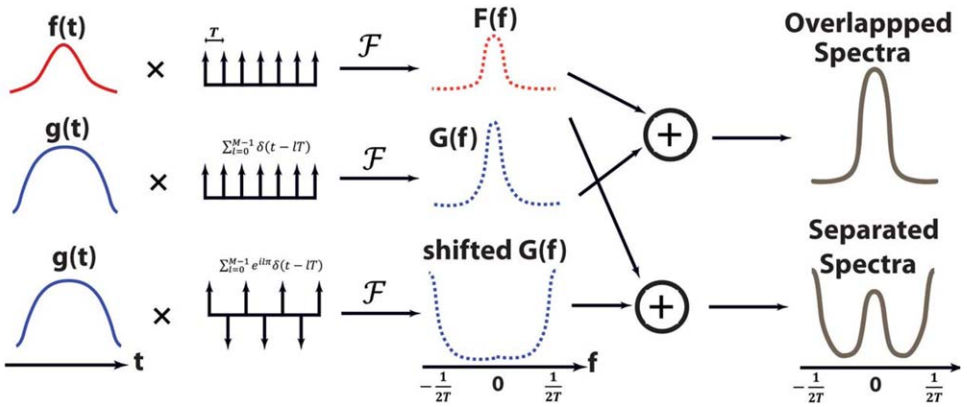

FIG. 1. Graphical representation of using temporal modulation to separate two functions. When sampling a composite function with two components, if the sampling function alternates polarity for one component, the spectra of the two components will be separate in the composite spectra.

acquired. The HOTSPA technique allows separations of the Fourier velocity spectrum (23) into components for the background phase (FC) waveform and the velocity waveforms along the three FE directions. Combinations of the acquired data enable 3D velocity calculations based on two acquired samples in the 3D space of gradient first moments (M_1) rather than four samples as in conventional 4D-flow techniques. We show that, compared with conventional 4D-flow, HOTSPA samples the hybrid M_1-t space more efficiently by shortening the temporal sampling period and temporal footprint of 4D-flow acquisitions by 50%. For conventional PC-MRI sequence with three FE directions and one FC measurement (FC/3FE), temporal sampling period = temporal footprint = 4*TR*VPS, and for our HOTSPA technique, temporal sampling period = temporal footprint = 2*TR*VPS. In vivo results show that the HOTSPA technique achieves more accurate peak velocity measurements than conventional 4D-flow, with no substantial compromise in total volumetric flow quantification accuracy, all achieved within a shorter total image acquisition time than conventional 4D-flow imaging.

THEORY

HOTSPA uses a temporal modulation technique to discriminate between two overlapping signals. Consider a generic composite time signal $h(t) = f(t) + g(t)$, in which $f(t)$ and $g(t)$. each has a spectral bandwidth B in the temporal frequency domain. In a conventional sampling strategy, the signal is sampled at certain time points specified by a sampling function $S(t) = \sum_{l=0}^{M-1}\delta(t - lT)$, such that $h(t)S(t) = \sum_{l=0}^{M-1}\delta(t - lT)f(t) + \sum_{l=0}^{M-1}\delta(t - lT)g(t)$, where $\delta(\cdot)$ is the delta function, M is the number of samples, and T is the sampling period. The digital Fourier transform on the sampled signal is shown in Eq. 1:

$$\mathcal{F}[h(t)S(t)] = \sum_{l=0}^{M-1}\delta\left(f - \frac{l}{T}\right) * F(f) + \sum_{l=0}^{M-1}\delta\left(f - \frac{l}{T}\right) * G(f). \quad [1]$$

In Eq. 1, $\mathcal{F}$ represents Fourier transform, $F(f) = \mathcal{F}[f(t)]$, $G(f) = \mathcal{F}[g(t)]$, and $*$ represents a convolution. It is clear that such a sampling strategy is not able to differentiate between $f(t)$ and $g(t)$, nor their respective spectra, as these two signals overlap in time and their spectra also overlap in the temporal frequency domain. However, we suppose that one can achieve a "special" sampling function $\tilde{S}(t)$ (it will be become clear later in the paper how this is achievable in PC-MRI), such that the polarity of the sampling function is alternated for signal $g(t)$ only as shown in Eq. 2:

$$h(t)\tilde{S}(t) = \sum_{l=0}^{M-1}\delta(t - lT)f(t) + \sum_{l=0}^{M-1}e^{il\pi}\delta(t - lT)g(t). \quad [2]$$

Compared with the sampling strategy $S(t)$ in Eq. 1, the sampling function in $\tilde{S}(t)$ for the $f(t)$ signal component remains the same as $S(t)$; however, the sampling function for the $g(t)$ signal component carries a linear phase ramp of π per sampling period T. According to Fourier sampling theory, if one performs a Fourier transform on the sampled function $h(t)\tilde{S}(t)$, the spectrum $G(f)$ will be shifted by $1/2T$, whereas $F(f)$ remains centered around zero frequency. Hence,

$$\mathcal{F}[h(t)\tilde{S}(t)] = \sum_{l=0}^{M-1}\delta\left(f - \frac{l}{T}\right) * F(f) + \sum_{l=0}^{M-1}\delta\left(f - \frac{1}{2T} - \frac{l}{T}\right) * G(f) \quad [3]$$

A graphical representation of Eq. 3 is shown in Figure 1, and it is clear that Fourier transform of the sampled signal enables one to completely discriminate between $f(t)$ and $g(t)$, as long as $T \leq \frac{1}{2B}$. In fact, one can obtain the spectrum $F(f)$ simply by taking the $\frac{M}{2}$ points around the zero frequency of the composite spectra in Eq. 3, and the remaining $\frac{M}{2}$ points correspond to the spectrum $G(f)$.

How to Achieve Temporal Modulation in HOTSPA PC-MRI Flow Encoding

The goal of a PC-MRI exam is to sample temporal FE signals in orthogonal spatial orientations. In a typical 4D PC-MRI exam, the FE phase in three orthogonal directions (i.e., *x, y,* and *z*) and the FC signal are required. For simplicity, we first consider a scenario in which only FE signal in two orthogonal directions are sampled. Without loss of generality, we suppose the FE directions are $\vec{e}_1 = \left(\frac{1}{\sqrt{2}}, \frac{1}{\sqrt{2}}\right) = (1 + \hat{\imath})/\sqrt{2}$ and $\vec{e}_2 = \left(\frac{1}{\sqrt{2}}, -\frac{1}{\sqrt{2}}\right) = (1 - \hat{\imath})/\sqrt{2}$, i.e., they are along the

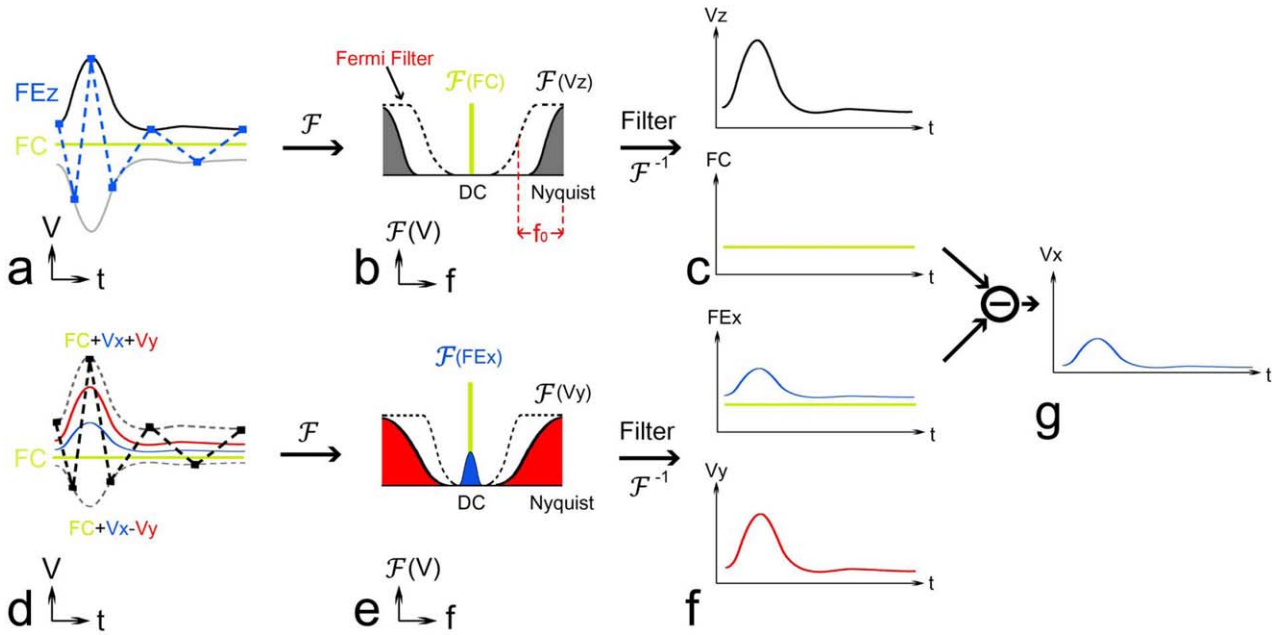

FIG. 2. (**a**) Two-sided FE_z without FC (Scenario 1) acquisition of HOTSPA (blue dash line) with alternating FE_z sampling. The positive and negative FE_z velocity waveform are shown in black and gray solid lines. The blue points are actual samples from the alternating sampling pattern. (**b**) Fourier transform of the signal sampled in (**a**). Fermi filter (black dash line) is applied to separate the two spectra. (**c**) Separated velocity waveforms of V_z and FC after filtering and inverse Fourier transform ($\mathcal{F}^{-1}$). (**d**) HOTSPA FE acquisition strategy for encoding two velocity directions V_x and V_y using a sampling function with alternating polarity for V_y sampling. The true flow waveforms of V_x and V_y are shown in blue and red solid lines. The composite waveform of FC + $V_x \pm V_y$ sampling is shown in dashed gray lines. The black samples are the actual acquired data using the alternating sampling pattern. (**e**) Fourier transform of the signal sampled in (d). Fermi filter is applied to separate the spectra of two velocities. The filter pass-band bandwidth is adapted based on relative magnitude/bandwidth of the V_x and V_y spectra. (**f**) Separated velocity waveforms V_y and FE_x after filtering and inverse Fourier transform ($\mathcal{F}^{-1}$). (**g**) Additional subtraction between FC and FE_x gives the V_x velocity waveform.

diagonal directions in the coordinate system spanned by the physical x - and y -axes. We further suppose the the velocity corresponding to a π FE phase (VENC) is the same for both FE directions, which is common in PC-MRI, and the physical x and y components of the velocity as a function of time are represented by $V_x(t)$ and $V_y(t)$, respectively. Hence the velocity can be represented in vector form as $\vec{V}(t) = V_x(t) + \hat{\imath} \cdot V_y(t)$. In typical PC-MRI, the FE direction alternates in time between $\vec{e}_1$ and $\vec{e}_2$. For $\vec{e}_1$ FE, the resultant phase accumulation caused by flow is shown in Eq. 4 as follows:

$$\phi_1(t) = \frac{\pi}{VENC}\vec{V}(t)\cdot\vec{e}_1 = \frac{\pi}{\sqrt{2}\cdot VENC}V_x(t) + \frac{\pi}{\sqrt{2}\cdot VENC}V_y(t). \quad [4]$$

Similarly, for $\vec{e}_2$ FE, the resultant phase accumulation is shown in Eq. 5:

$$\phi_2(t) = \frac{\pi}{VENC}\vec{V}(t)\cdot\vec{e}_2 = \frac{\pi}{\sqrt{2}\cdot VENC}V_x(t) - \frac{\pi}{\sqrt{2}\cdot VENC}V_y(t). \quad [5]$$

Note the $V_x(t)$ portion of the velocity is encoded positively, regardless of $\vec{e}_1$ or $\vec{e}_2$ FE; however, the polarity of $V_y(t)$ velocity encoding is alternated between $\vec{e}_1$ and $\vec{e}_2$ FE directions. Based on the aforementioned temporal modulation theory, the alternating FE pattern of $\vec{e}_1$ or $\vec{e}_2$ sampling is equivalent to applying the "special" sampling function $\tilde{S}(t)$, scaled by $\frac{\pi}{\sqrt{2}\cdot VENC}$ (24), to a hypothetical composite time signal $h(t) = V_x(t) + V_y(t)$. Therefore, by applying a temporal Fourier transform to our measurements, which includes alternating FE directions, the spectrum for $V_x(t)$ will be centered around zero frequency, whereas the spectrum for $V_y(t)$ will be shifted by $\frac{1}{2T}$, half of the frequency support (Fig. 2e). Under our assumption so far that $T \leq \frac{1}{2B}$ (in practice, this assumption is not valid, which will be discussed later in the paper), these two spectra will have no overlap and can easily be differentiated.

Asymmetric Spectra

Compared with the conventional PC-MRI, our temporal modulation scheme doubles the temporal sampling rate and spectral support in the frequency domain, and shortens the temporal footprint for each cardiac phase by 50%. Furthermore, for scenarios in which the two spectra require different spectral support, our temporal modulation technique can provide benefits in addition to the shorter temporal footprint, as it has the flexibility to asymmetrically allocate spectral support that is appropriate for each velocity component. We describe two such scenarios of asymmetric spectra in our HOTSPA PC-MRI.

Scenario 1: Two-Sided FE without FC

Let us consider the application of our temporal modulation approach to a conventional 2D PC-MRI experiment

acquired with VPS = 1, in which the FC and $V_z(t)$ (through-plane component of the velocity) data are sampled in an interleaved fashion. Hence, the data for each cardiac phase is acquired within two TRs. We compare this with a two-sided FE strategy in which only the $V_z(t)$ data are sampled with alternating FE polarity, as shown in Figure 2a. Such a 2D PC-MRI acquisition strategy is the same as the SVE technique (5). The phase for the acquired FE_z signal $\phi_z(t)$ is therefore $\phi_0(t) + \phi_{v,z}(t)$ for odd cardiac phases and $\phi_0(t) - \phi_{v,z}(t)$ for even cardiac phases, where $\phi_0(t)$ is the the FC background phase and $\phi_{v,z}(t)$ is the signal phase associated with $V_z(t)$. Based on the aforementioned temporal modulation theory, if one performs a temporal Fourier transform of $\phi_z(t)$, there will be two separate spectra: 1) the spectrum for $\phi_0(t)$, which occupies the lower frequency (near DC) region; and 2) the spectrum of $\phi_{v,z}(t)$, which will be shifted by half of the spectral support because of the alternating 0–180° phase modulations (25) of the $\phi_{v,z}$(t) waveform. Based on previous studies (6), the FC background phase is not expected to change quickly over time; therefore, the spectrum for $\phi_0(t)$ will have a narrower bandwidth compared with $\phi_{v,z}$ (t) and requires a small spectral support. Figures 2a–2b demonstrates a simplified/extreme case in which the FC phase is constant during the cardiac cycle, which corresponds to a delta function in the frequency domain. In this extreme case, we can allocate the entire spectral support for $V_z(t)$ (except the single delta function at zero temporal frequency). In this scenario, the fact that the FC and $V_z(t)$ data require asymmetric spectral support enables our temporal modulation approach to double the temporal resolution for $V_z(t)$ compared with conventional PC-MRI; however, in conventional 2D PC-MRI, one is forced to assign the same spectral support for both the FC and the FE_z signal, despite the fact that the FC data do not require such a wide spectral support.

Scenario 2: Diagonal Velocity

In the example shown in Eqs. 4 and 5, suppose $V_y(t) = 0$, i.e., the true velocity is along the direction of $\vec{e}_1 + \vec{e}_2$ (i.e., the physical x -axis), then the spectrum for $V_y(t)$ requires no spectral support and the entire spectral support can be allocated retrospectively for the $V_x(t)$ spectrum. In this case, the true temporal resolution is doubled for those voxels with this diagonal velocity or with velocity that is closely aligned along the $\vec{e}_1 + \vec{e}_2$ direction. This benefit is clear from the temporal sampling domain. Each FE datum, regardless of whether it is $\vec{e}_1$ FE or $\vec{e}_2$ FE sampling, effectively only samples $V_x(t)$, as $V_y(t)$ does not contribute to these FE data; hence, each $\vec{e}_1$ or $\vec{e}_2$ FE datum should be treated as an independent cardiac phase, as is the case in our temporal modulation scheme. However, if the conventional PC-MRI processing was employed, each pair of $\vec{e}_1$ and $\vec{e}_2$ FE data would have been forced to be lumped into a single cardiac phase that is twice as long, and the calculated $V_x(t)$ would effectively be an average between the velocities at the time point of $\vec{e}_1$ and $\vec{e}_2$ FE sampling. The same benefit is also achievable for voxels with velocity along the $\vec{e}_1 - \vec{e}_2$ direction, i.e., the other diagonal velocity direction with nonzero $V_y(t)$ and $V_x(t) = 0$. In reality, the $V_x(t)$ or $V_y(t)$ velocities are typically not strictly zero. However, as long as one of them does not contribute significantly to the signal (i.e., the velocity direction is approximately along one of the two diagonal velocity directions), then we achieve improved temporal resolution using the temporal modulation. We note that even for velocities not along one of the two diagonal velocity directions, the temporal modulation technique still would be more accurate than conventional PC-MRI, because although both techniques would have the same spectral support for both directions, the temporal footprint of HOTSPA would be shorter.

Temporal Filtering

We now revisit the generic composite signal $h(t) = f(t) + g(t)$ and the composite spectra $H(f) = \mathcal{F}[h(t)S(t)]$. The two spectra $F(f)$ and $G(f)$ are completely separate with no overlap if $T \leq \frac{1}{2B}$. However, in PC-MRI, this Nyquist sampling condition is rarely satisfied in the strict sense, as the acquisition time available for PC-MRI, especially for 4D-flow, typically limits the sampling rate to below the true Nyquist rate. When $\frac{1}{2B} \leq T \leq \frac{1}{B}$, which means spectra $F(f)$ and $G(f)$ will overlap each other to a degree that depends on T, we need to implement a temporal filter to best separate the two partially overlapped spectra automatically for each voxel. The goal of the filter is twofold: 1) for scenarios in which both spectra within $H(f)$ are comparable with respect to magnitude and bandwidth (eg, for voxels with velocity along the $\vec{e}_1$ or $\vec{e}_2$ FE direction), the filter needs to allocate approximately equal spectral support for the two spectra; 2) for either one of the "asymmetric spectra" scenarios in the previous section, the filter needs to allocate automatically a larger spectral support for the more significant component of the composite spectra.

There are many possible filter designs that can satisfy our requirement. In our present work, we empirically chose a Fermi filter $K(f)$ (17) that is centered at the higher peak of the composite spectra (Fig. 2b dash lines):

$$K(f) = \frac{1}{1 + \exp\left(\frac{f - f_0}{C}\right)}. \quad [6]$$

In Eq. 6, the constant C controls the shape of the Fermi filter and we empirically chose $C = 0.22$. f represents temporal frequency, and f_0 is the frequency corresponding to 50% of the full width half maximum (FWHM) for the Fermi filter (Fig. 2b). In this work, the Fermi filter parameter f_0 was determined automatically on a voxel-by-voxel basis by the following steps: 1) Identify the maximum and minimum points in $H(f)$: $f_{max} = \text{argmax}_f \{H(f)\}$ and $f_{min} = \text{argmin}_f \{H(f)\}$; 2) identify the set of points in $H(f)$ according to Eq. 7 as follows:

$$c = \Big\{ f \mid H(f) < \frac{\max[H(f)] - \min[H(f)]}{10} + \min[H(f)] \ \&\ abs(f - f_{max}) \geq \frac{1}{4T} \Big\}; \quad [7]$$

3) identify the following point from set $\mathbb{C}$: $f_b = \{f \in \mathbb{C} \mid \forall a \in \mathbb{C} : abs(f - f_{max}) \leq abs(a - f_{max})$; and 4) Set the f_0 parameter of the Fermi filer $K(f)$ as $f_0 = abs(f_{max} - f_b)$

and apply the filter to $H(f)$ centered around f_{max}. When applying this temporal filtering technique to our HOTSPA PC-MRI signal shown in Eqs. 4 and 5, the result of the filtering will be the spectrum for $V_y(t)$ (higher peak in Fig. 2e), and the residual spectrum after filtering will be the spectrum for $V_x(t)$ (lower peak in Fig. 2e). As the location of the f_b point depends on the relative strength of the two partially separated spectra, our Fermi temporal filter is capable of adaptively allocating pass-band bandwidth for each spectrum on a voxel-by-voxel basis without manual interference. In many vessel territories, one could orient the FE directions along two orthogonal directions that are 45° from the predominant blood flow direction to take advantage of the wider spectral support in these velocity directions. In comparison, conventional 4D-flow PC-MRI does not have this benefit, as the FE data in each of the three orthogonal directions, regardless of the actual blood flow direction and presence/absence of significant flow component in the *x, y*, and *z* direction(s), are forced to allocate the same spectral support corresponding to the temporal sampling period of $4 \times \mathrm{VPS} \times \mathrm{TR}$.

HOTSPA 4D-Flow

We now put the aforementioned theory together and consider the HOTSPA 4D-flow MRI method shown in Figure 3. For the $\mathrm{VPS} = 1$ case, each cardiac phase contains data from two TRs: one for the $\pm \mathrm{FE_z}$ encoding and one for FE in two orthogonal directions in the *x*-*y* plane (i.e., $\vec{e}_1$ and $\vec{e}_2$). In the first step of the HOTSPA reconstruction, we separate the $V_z(t)$ and background FC data $\phi_0(t)$ by applying our temporal filtering to the $\pm\mathrm{FE_z}$ data only (as shown in Figs. 2a–2c). In the second step, another temporal filtering is applied in the Vx-Vy composite spectra to separate $\mathrm{FE_x}$ and $V_y(t)$ data. Finally, the $\phi_0(t)$ data are subsequently subtracted from the $\mathrm{FE_x}$ data (as shown in Figs. 2f–2g).

Although in this work we focus on validation of HOTSPA for PC-MRI with three orthogonal FE directions, the same approach may be applied to four-point balanced PC-MRI sampling (i.e., tetrahedral M_1 space sampling). Typical four-point balanced PC-MRI sequentially acquires $\phi_0 + \phi_x + \phi_y + \phi_z$, $\phi_0 - \phi_x - \phi_y + \phi_z$, $\phi_0 - \phi_x + \phi_y - \phi_z$, and $\phi_0 + \phi_x - \phi_y - \phi_z$. We can apply HOTSPA in two separate stages. First we define the following four functions:

$$f(t) = \phi_0 + \phi_y \quad g(t) = \phi_z + \phi_x$$
$$f'(t) = \phi_0 - \phi_y \quad g'(t) = \phi_z - \phi_x$$

Hence, the four-point balanced PC-MRI samples the following flow waveforms:

$$f(t) + g(t) \quad f'(t) + g'(t)$$
$$f(t) - g(t) \quad f'(t) - g'(t)$$

From the $f(t) + g(t)$ and $f(t) - g(t)$ data, we can separate the spectra for $f(t)$ and $g(t)$ using our HOTSPA temporal filtering; from the $f'(t) + g'(t)$ and $f'(t) - g'(t)$ data, we can similarly separate the spectra for $f'(t)$ and $g'(t)$. After we have solved for all four velocity waveforms, two additional HOTSPA temporal filtering can be applied—one for the alternating pattern of $f(t) = \phi_0 + \phi_y$ and $f'(t) = \phi_0 - \phi_y$ to separate the ϕ_0 and ϕ_y spectra, and the other filter for the alternating pattern of $g(t) = \phi_z + \phi_x$ and $g'(t) = \phi_z + \phi_x$ to separate the ϕ_z and ϕ_x spectra. In the four-point balanced PC-MRI case, all of the aforementioned benefits of HOTSPA still hold.

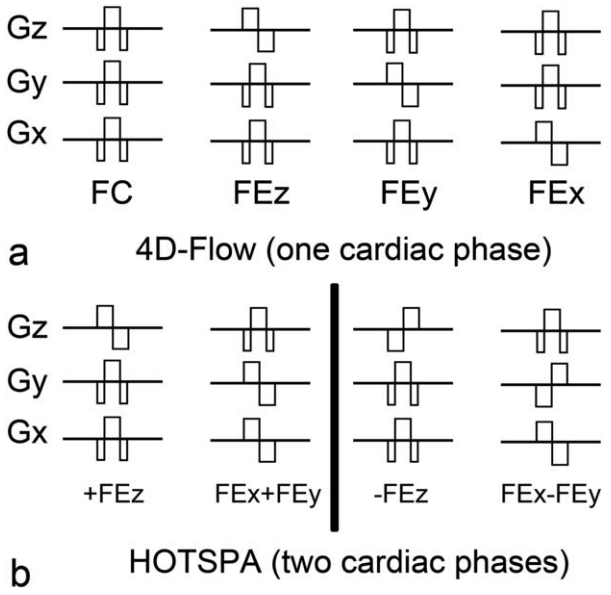

FIG. 3. Sequence diagrams of conventional 4D-flow acquisition (**a**) and HOTSPA acquisition (**b**). For each cardiac phase, 4D-flow requires four samples, whereas HOTSPA requires only two samples. In the diagrams, only FC (three gradients) and ±FE gradients (bipolar gradients) are shown.

METHODS

Our institutional review board approved this study. Informed consent was obtained from all study participants. All studies were performed on a 3 Tesla (T) scanner (Skyra, Siemens, Germany) using a 4-channel neck coil and 18-channel torso coil for in vivo studies. Eddy current correction was applied in all of the in vivo studies data sets by subtracting the phase images of a steady phantom, repeating scans with the same parameters from the in vivo scans.

Numerical Simulation

Numerical simulation was performed to study the accuracy of HOTSPA in comparison with conventional PC-MRI and the dependence of HOTSPA flow quantification accuracy on the angle ψ. between the flow direction and the physical *x*-axis. As shown in Figure 4a, we created a single 2D slice numerical phantom with elliptical stationary tissue (gray) and blood vessels (white). To simplify the simulation, we assume every voxel within the blood vessels has the same velocity, the blood only flows within the 2D imaging slice (i.e., no through-plane flow), and the velocity magnitude (in units of cm/s) strictly follows the Gaussian function in Eq. 8:

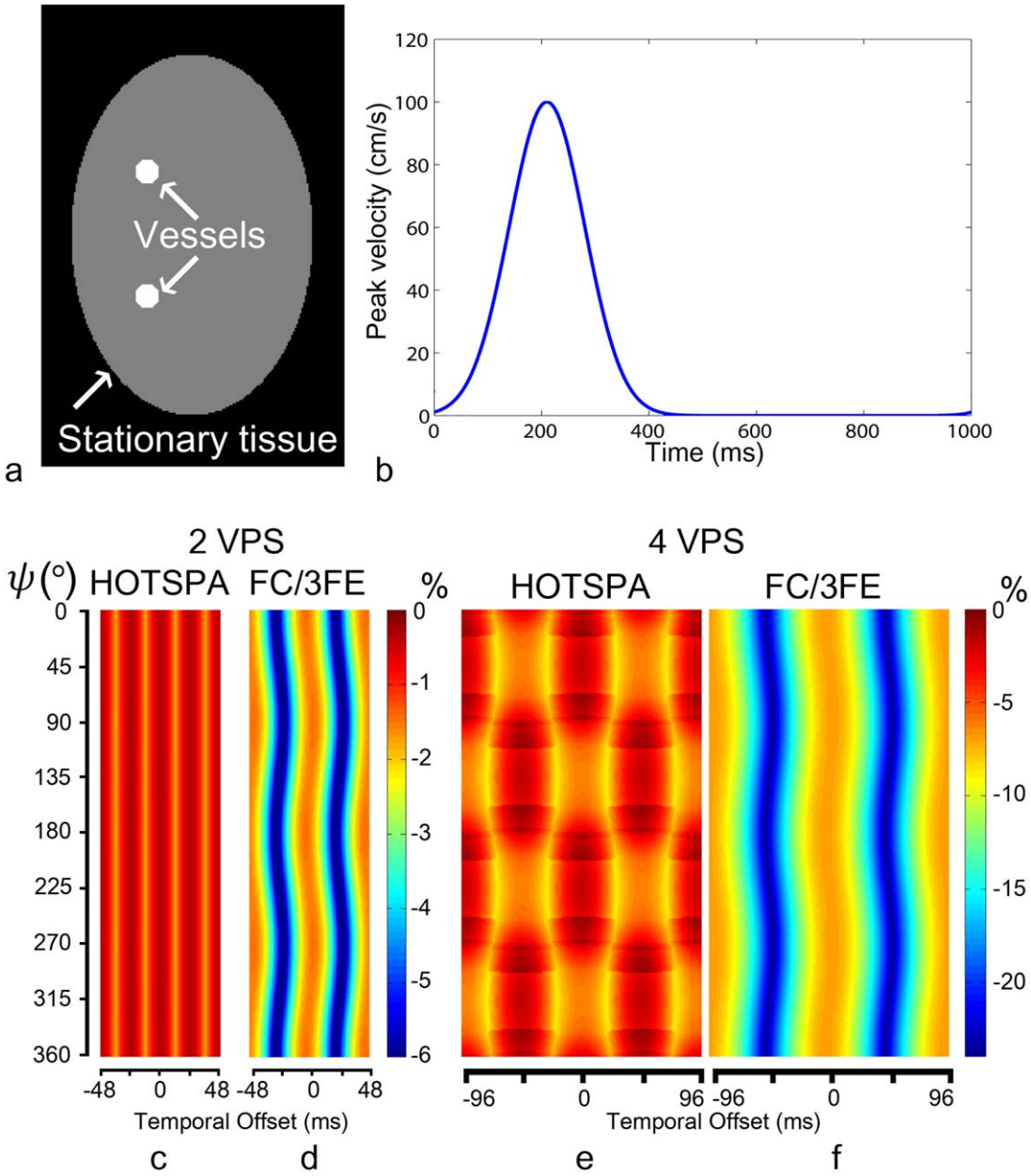

FIG. 4. Computer simulation: (**a**) Magnitude image of simulated object. (**b**) Ground truth velocity magnitude waveform. (**c** and **d**) Peak velocity measurement error maps of 2-VPS HOTSPA and FC/3FE as a function of the ψ angle (0–360°) and the temporal offset (−48 to 48 ms). (**e** and **f**) Peak velocity measurement error maps of 4-VPS HOTSPA and FC/3FE as a function of the ψ angle (0–360°) and the temporal offset (−96 to 96 ms).

$$V_{sim}(t) = 100e^{-\frac{(t-210)^2}{2\times 70^2}}. \quad [8]$$

In Eq. 8, t is the time in milliseconds within the simulated cardiac cycle of 1000 ms. We simulated the entire cardiac phase-resolved k-space data for a conventional 4D-flow sequence and our HOTSPA 4D-flow sequence with the following parameters: TR/echo time (TE) = 6/4 ms, VENC = 200 cm/s, matrix = 256 × 176, and VPS = 2 and 4. The simulated FE directions were physical x- and y-axes for the conventional sequence and the two diagonal directions in the x-y plane (i.e., $\vec{e}_1$ and $\vec{e}_2$) in the HOTSPA. The goal of our simulation is to study the dependence of peak velocity estimation accuracy on the following two factors: 1) the angle ψ ; and 2) the temporal offset between the true peak and sample points (5). To achieve this goal, we simulated 360 ψ angles (1° to 360°) and temporal offsets within the range of ± 4*TR*VPS. For HOTSPA, we performed the aforementioned temporal filtering to separate the $V_x(t)$ and $V_y(t)$ signal, which were subsequently combined. For the simulated conventional 4D-flow k-space data sets, the conventional phase-contrast reconstruction was performed. The peak velocities calculated from these simulated k-space data sets were compared with the ground truth from Eq. 8.

Table 1
Sequence Parameters (Both HOTSPA and FC/3FE) for In Vivo Studies

	2D in vivo study (carotid)	4D in vivo study (carotid)	2D in vivo study (aorta)
TR (ms)	6.3	6.2–6.4	5.2–5.4
TE (ms)	3.9	3.6–3.9	3.2–3.4
Flip angle (°)	20	20	20
Readout BW (Hz/Pixel)	500	815	500
VENC (cm/s)	100–110	100–110	120
VPS	1 and 2 (FC/3FE) 2 (HOTSPA)	4	2 (FC/3FE) 4 (HOTSPA)
Acquired matrix size	256 × 176	256 × 176 × 8	128 × 88
FOV (mm)	256 × 176	256 × 176 × 20	256 × 176
Slice thickness (mm)	7	2.5	7
Acceleration factor	Fully sampled	Fully sampled	3x GRAPPA (24 autocalibration lines)

In Vivo Study

The HOTSPA acquisition strategy was implemented for a 3T MRI system (Skyra, Siemens Medical Solutions). Six volunteers (ages 27 ± 3 years) were scanned at the common carotid arteries (CCAs) using two sequences: 1) conventional PC-MRI with 2D spatial encoding but with three FE directions plus the FC data, i.e., 2D FC/3FE; and 2) our HOTSPA strategy but with 2D spatial encoding, i.e., 2D HOTSPA. The sequence parameters are listed in Table 1 under "2D in vivo study (carotid)." The average total acquisition times of the three scans were 179 s (range: 124–206 s) for 1-VPS 2D FC/3FE, 87 s (range: 59–99 s) for 2-VPS FC/3FE, and 86 s (range: 60–103 s) for 2D HOTSPA. The imaging plane of each data set was at approximately 50° (instead of 90°) relative to the longitudinal axis of the CCAs, so that the velocity has significant components in more than one direction (as shown in Fig. 5a).

After the 2D study, six additional adult volunteers were scanned at the CCAs using the FC/3FE with 3D spatial encoding (i.e., 4D FC/3FE) and our HOTSPA sequence with 3D spatial encoding (4D HOTSPA). The sequence parameters are listed in Table 1 under "4D in vivo study (carotid)." The average total acquisition time of the two scans was 7 min 57 s (range: 6 min 54 s–9 min 5 s) for 4D FC/3FE and 7 min 24 s (range: 5 min 22 s–8 min 54 s) for 4D HOTSPA. For each 4D data set, three slices (slice 2, 4, and 6 along slab direction) were selected to compare the total volumetric flow and peak velocity measurements.

To demonstrate the benefits of our HOTSPA technique in the thorax, one additional volunteer was scanned at the ascending aorta using both the 2D FC/3FE and the 2D HOTSPA sequences. Both sequences were implemented with parameters listed in Table 1 under "2D in vivo study (aorta)." The imaging plane of each data set was perpendicular to the ascending aorta. The total acquisition times were 27 s for 2D FC/3FE and 16 s for 2D HOTSPA. The scan was acquired during a breathhold with prospective electrocardiogram gating.

RESULTS

Numerical Simulation

As shown in Figs. 4c–4f, the peak velocity estimation accuracy of HOTSPA and conventional FC/3FE were both dependent on the ψ angle and the temporal offset μ. For 2-VPS simulation (Figs. 4c–4d), for the entire range of temporal offset μ and ψ angle, the peak velocity estimation errors ranged from -1.8 to -0.4% for HOTSPA and ranged from -7.0 to -1.5% for FC/3FE. When comparing the HOTSPA with FC/3FE 4-VPS simulation results (Figs. 4e–4f), for all of the ψ and μ combinations, the HOTSPA error was between -8.9 and -0.7%, whereas the FC/3FE error was between -23.9 and -6.9%. If we compare the HOTSPA and FC/3FE accuracy for any given μ, the HOTSPA error was always smaller than FC/3FE, regardless of the ψ angle. The HOTSPA accuracy is greatly improved when ψ is within $\pm 15^\circ$ around the physical x- or y-axes (i.e., $\psi = 0^\circ,\ 90^\circ, 180^\circ, 270^\circ$). This is because these velocity directions correspond to the "diagonal velocity" in the aforementioned Scenario 2 and the HOTSPA Fermi filter automatically allocates a larger spectral support for these velocities, which translates to more accurate peak velocity magnitude estimation. For velocities that are approximately along the $\vec{e}_1$ or $\vec{e}_2$ FE direction (e.g., when $\psi \approx 135^\circ$ and $\mu = 0$), the HOTSPA error was generally between 5 and 10%. We note that the HOTSPA error was also small (<5%) when the velocity is along $\vec{e}_1$ or $\vec{e}_2$ and the $\vec{e}_1$ or $\vec{e}_2$ FE sampling falls on the ground truth peak location (e.g., when $\psi \approx 45^\circ$ and $\mu = 0$ or when $\psi \approx 135^\circ$ and $\mu = \pm 48$ ms). This is because, although the Fermi filter does not allocate a larger spectral support for these velocities, the single FE sample itself would already be sufficient to provide accurate peak velocity estimation. Therefore, the HOTSPA technique is always more accurate than the conventional FC/3FE technique—regardless of the velocity direction. For certain velocity directions it is slightly better, and for certain other directions it reduced the peak velocity estimation error by several fold.

In Vivo Study

Figures 5b–5c show examples of through-plane mean velocity and peak velocity measurement (average and maximum within the vessel lumen, respectively) of the CCA comparing three different measurements: 1) the 1-VPS 2D FC/3FE (gray) with 25.12 ms temporal sampling period; 2) the 2-VPS 2D HOTSPA (blue) with 25.12 ms temporal sampling period; and 3) the 2-VPS 2D FC/3FE PC-MRI (red) with 50.24 ms temporal sampling period. The velocity measurements (both through-plane mean

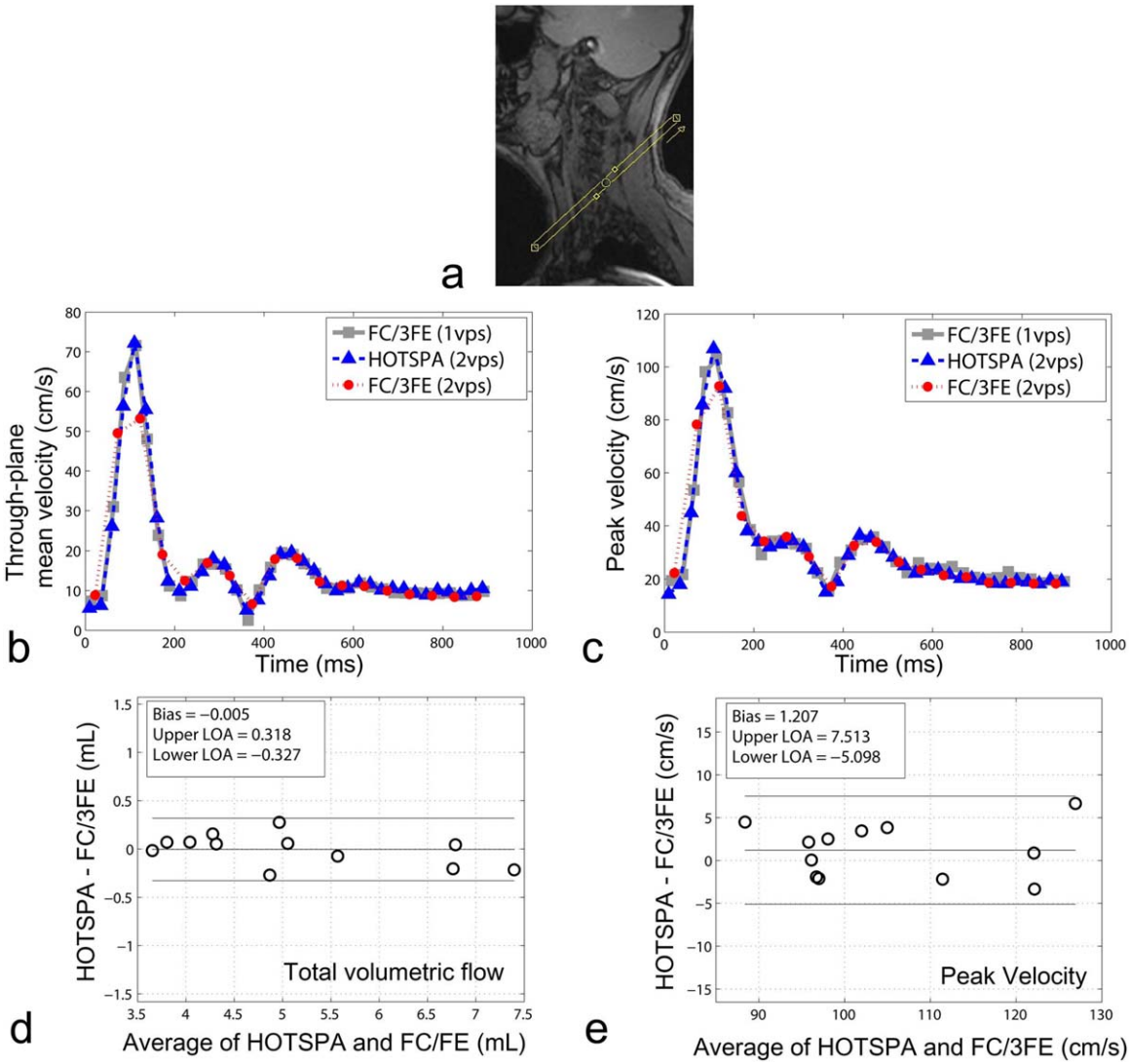

FIG. 5. (**a**) Localizer image of a volunteer. 2D in vivo results. (**b**) Through-plane mean velocity waveforms of the reference 1-VPS 2D FC/3FE (gray), 2-VPS HOTSPA (blue), and 2-VPS 2D FC/3FE PC-MRI (red). (**c**) Peak velocity waveforms of the reference 1-VPS FC/3FE (gray), 2-VPS HOTSPA (blue), and 2-VPS FC/3FE (red). (**d**) Bland-Altman plot of total volumetric flow measurements between 1-VPS FC/3FE and 2-VPS HOTSPA. (**e**) Bland-Altman plot of peak velocity measurements using 1-VPS FC/3FE PC-MRI and 2-VPS HOTSPA. The 2-VPS HOTSPA provides accurate mean and peak velocity using the 1-VPS conventional FC/3FE as the reference, while saving 50% in scan time. The 2-VPS FC/3FE significantly underestimated the peak velocity.

velocity and peak velocity) were similar between the 2-VPS 2D HOTSPA and the 1-VPS 2D FC/3FE, although the HOTSPA acquisition time was reduced by 50%. However, 2D FC/3FE with VPS = 2 underestimated the peak velocity by approximately 15% because of its long temporal footprint and temporal sampling period. Across the six subjects, using the 2D 1-VPS FC/3FE as the reference, the bias of 2D HOTSPA was −0.005 mL (−0.1% relative bias error) with 95% confidence interval (CI) [−0.3, 0.3] mL for total volumetric flow and 1.21 cm/s (1.14% relative bias error) with 95% CI [−5.1, 7.5] cm/s for peak velocity (Bland-Altman plots of Figs. 5d–5e). The peak velocity of all 12 measurements based on the 2-VPS HOTSPA and 1-VPS 2D FC/3FE PC-MRI were significantly higher than the 2-VPS 2D FC/3FE measurements (104.5 ± 12.7 cm/s for 1-VPS 2D FC/3FE, 105.7 ± 12.7 cm/s for 2-VPS 2D HOTSPA, and 90.6 ± 10.6 cm/s for 2-VPS 2D FC/3FE, $P < 0.05$, one-side paired t-test).

Figures 6a–6b show an example of through-plane mean velocity and peak velocity in one slice of the 4D-flow data comparing two different measurements: 1) the 4-VPS 4D FC/3FE shown in red with 98.08 ms temporal sampling period; and 2) the 4-VPS 4D HOTSPA technique (blue) with 51.36 ms temporal sampling period. The 4D HOTSPA technique generated up to 40% higher peak velocity compared with standard 4D FC/3FE. As shown in Figure 6c, the total volumetric flow measurements agree well between 4D HOTSPA and 4D FC/3FE (−0.02 mL bias with [−0.3, 0.3] mL 95% CI). The peak velocity from 4-VPS HOTSPA (average = 98.0 cm/s, range: 73.7–125.6 cm/s) was significantly higher than the 4-VPS standard FC/3FE 4D-flow (average = 83.2 cm/s, range: 60.2–109.6 cm/s) ($P < 0.05$, one-sided paired t-test).

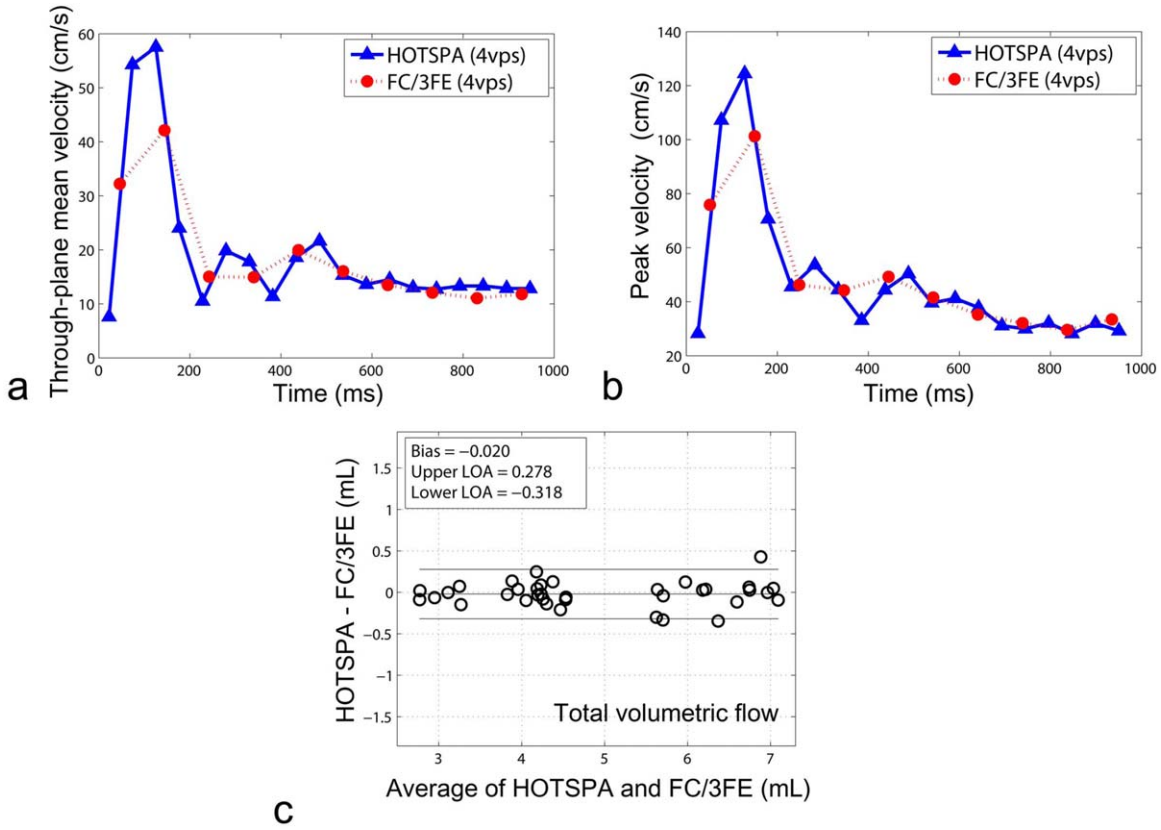

FIG. 6. Example of through-plane mean velocity waveforms (**a**) and peak velocity waveforms (**b**) of one selected slice from the 4-VPS conventional FC/3FE 4D-flow (red) with 98.08 ms temporal sampling period, and 4-VPS 4D HOTSPA (blue) with 51.36 ms temporal sampling period. Both sequences had the same total scan time. The peak velocity calculated from the 4D HOTSPA was $>20\%$ higher than that calculated from the FC/3FE. (**c**) Bland-Altman plot of total volumetric flow measurements (slice 2, 4, and 6 of both CCAs of all six volunteers) between conventional FC/3FE 4D-flow and 4D HOTSPA.

Figures 7a–7b show the mean velocity and peak velocity measured at the ascending aorta in one volunteer. The 4-VPS 2D HOTSPA provided similar mean and peak velocity measurements with the 2-VPS 2D FC/3FE, although the HOTSPA acquisition time was only 50% of the FC/3FE. The total volumetric flow was 100.8 mL based on FC/3FE, and 102.5 mL based on HOTSPA (1.7% difference). The peak velocity was 102.4 cm/s based on FC/3FE, and 102.8 cm/s based on HOTSPA (0.4% difference).

DISCUSSION

In this work, we propose a new flow-encoding and velocity calculation strategy for 4D-flow MRI with improved temporal sampling period and reduced temporal footprint using temporal modulation of the flow-encoding gradient waveforms. In our HOTSPA technique, the four acquisitions (FC and three FE directions) needed for conventional FC/3FE PC-MRI have been reduced to two acquisitions with alternating encoding

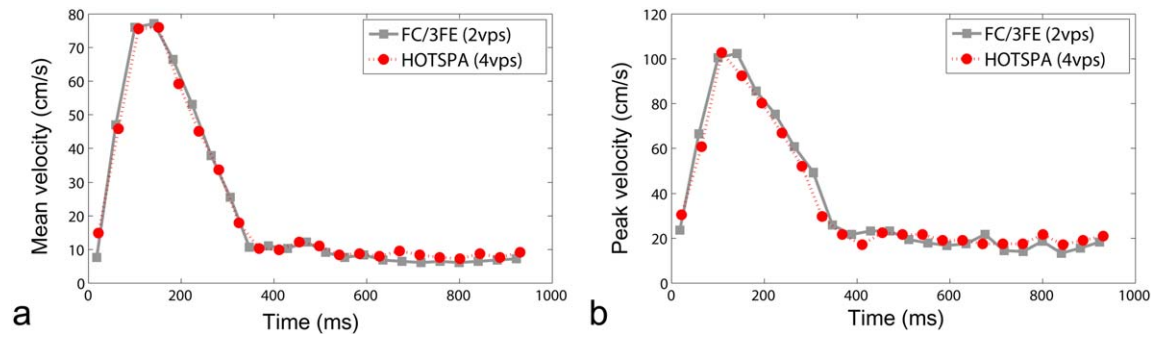

FIG. 7. Example of ascending aorta scan in a healthy volunteer. (**a**) Mean velocity comparison between 2-VPS FC/3FE (gray) and 4-VPS HOTSPA (red). (**b**) Peak velocity comparison between 2-VPS FC/3FE (gray) and 4-VPS HOTSPA (red). The 4-VPS HOTSPA provides similar mean and peak velocity measurements as 2-VPS FC/3FE, while reducing the scan time by 50%.

polarities for two of the three orthogonal FE directions between two successive cardiac phases. This was feasible because the temporal modulation of the FE directions shifts the Fourier spectrum of the velocity waveform for the direction with alternating polarity, which enables separation of the spectra for all three FE directions using a temporal frequency filter. Conventional PC-MRI velocity calculations are typically performed separately for each cardiac phase, and recent k-t acceleration methods focus on performing a temporal modulation of sampling pattern in an undersampled k-t-space. To the best of our knowledge, this is the first study to examine a temporal modulation strategy for an undersampled M_1 space. Compared with conventional PC-MRI, HOTSPA has the following advantages: 1) It enables a 50% shorter temporal footprint for each cardiac phase, which translates to more accurate peak velocity measurements while maintaining the measurement accuracy for total volumetric flow; and 2) it permits a flexible temporal filter spectral bandwidth on a voxel-by-voxel basis to achieve better accuracy for certain velocity directions, whereas conventional PC-MRI effectively forces each FE direction to use the same spectral bandwidth, regardless of whether there is significant flow in that FE direction for a given voxel. Furthermore, the temporal filter bandwidth for each FE direction can be retrospectively determined for a given voxel, based on the actual acquired composite spectra for that voxel. It should be noted that HOTSPA can be combined with other acceleration methods, such as parallel imaging and compressed sensing, to further accelerate data acquisition.

The HOTSPA technique enables a more flexible choice of temporal sampling period. The temporal sampling period and footprint of HOTSPA is equal to 2*TR*VPS, whereas the conventional 4D-flow is equal to 4*TR*VPS. For example, in our 2D PC-MRI experiments, HOTSPA allows for 12.5, 25, 37.5, and 50 ms temporal sampling period and temporal footprint selection; however, conventional 2D FC/3FE PC-MRI can enable only 25 and 50 ms (or greater) choices. In a hypothetical application that needs a 40-ms temporal sampling period, the conventional FC/3FE would have to choose one VPS with a 25 ms temporal sampling period to maintain the measurement accuracy, whereas HOTSPA would be able to use three VPS with 37.5 ms temporal sampling period.

Although the benefit of HOTSPA in two-sided FE without FC (Scenario 1) is clear, its benefit in flow encoding two orthogonal directions warrants further discussion. In these cases, the two spectra will likely overlap in practice and make it difficult to apply our filter without reducing temporal fidelity of the flow velocity data. However, overlapping spectra in our HOTSPA composite spectra indicates that a conventional PC-MRI acquisition with the same VPS does not satisfy Nyquist rate either and will suffer from similar loss in temporal fidelity because of frequency aliasing. Therefore, HOTSPA should not do worse than conventional PC-MRI in this regard. In addition, regardless of whether the Nyquist sampling rate is satisfied, the temporal footprint of HOTSPA for each cardiac phase is 50% of conventional PC-MRI. Consider a HOTSPA acquisition with 25 ms temporal footprint for each cardiac phase and a conventional PC-MRI with the same VPS and 50 ms temporal footprint. In the conventional PC-MRI reconstruction, we treat the $V_x(t)$ and $V_y(t)$ encoding data as if they were acquired at the same instant within the long 50 ms window, whereas in fact they are not. Our HOTSPA recognizes this fact and treats the e_1 FE data as if they were acquired at an instant within 0–25 ms and the e_2 FE data as if they were acquired at an instant between 25–50 ms. This effect of shorter temporal footprint results in better peak velocity measurement accuracy using HOTSPA, and is reflected in our numerical simulation results shown in Figure 4. Furthermore, for the diagonal velocity directions (Scenario 2), the HOTSPA provides more accurate peak velocity measurements as a result of our adaptive filter bandwidth. Our numerical simulation results in Figure 4 show that for voxels with these diagonal velocity directions, HOTSPA provides better accuracy by adaptively allocating a larger bandwidth for the dominant velocity. In these cases, the magnitudes of the two spectra differ greatly, such that the nondominating spectrum becomes negligible relative to the dominant spectrum and is irrelevant in our velocity calculation—although it might have a large bandwidth and overlap with the dominant spectrum. In summary, our HOTSPA should always provide more velocity measurement accuracy compared with conventional PC-MRI, because of its shorter sampling period. For certain velocity directions, the accuracy benefit is greater than voxels with some other velocity directions, but the accuracy benefits are always obtainable regardless of the velocity direction.

Our work has limitations. First, because our main goal was to introduce the HOTSPA concept and demonstrate its preliminary feasibility, we did not thoroughly evaluate the velocity-to-noise ratio (VNR) of our technique, which is particularly important for calculating hemodynamic parameters such as pressure gradient and wall shear stress. We speculate that the HOTSPA VNR will be reduced by $\sqrt{2}$ fold (24) compared with conventional PC-MRI for the diagonal velocity case in Scenario 2. This is because the effective VENC along the velocity direction is multiplied by $\sqrt{2}$ as evidenced by the $\frac{\pi}{\sqrt{2}\cdot VENC}$ scale factor in Eqs. 4 and 5. Nevertheless, the VNR aspect of the HOTSPA warrants further systematic study. Second, as a feasibility study, the current work lacks validation of the technique in different vascular territories. Third, our work is only tested in a small number of healthy volunteers and in vivo validation in patients with hemodynamic abnormalities and various forms of flow patterns need to be performed.

REFERENCES

1. Pelc NJ, Herfkens RJ, Shimakawa A, Enzmann DR. Phase contrast cine magnetic resonance imaging. Magn Reson Q 1991;7:229–254.
2. Jung B, Markl M, Föll D, Hennig J. Investigating myocardial motion by MRI using tissue phase mapping. Eur J Cardiothorac Surg 2006;29:S150–S157.
3. Markl M, Rustogi R, Galizia M, Goyal A, Collins J, Usman A, Jung B, Foell D, Carr J. Myocardial T2-mapping and velocity mapping: changes in regional left ventricular structure and function after heart transplantation. Magn Reson Med 2013;70:517–526.

4. Markl M, Frydrychowicz A, Kozerke S, Hope M, Wieben O. 4D-flow MRI. J Magn Reson Imaging 2012;36:1015–1036.
5. Lin H-Y, Bender JA, Ding Y, Chung Y-C, Hinton AM, Pennell ML, Whitehead KK, Raman SV, Simonetti OP. Shared velocity encoding: a method to improve the temporal resolution of phase-contrast velocity measurements. Magn Reson Med 2012;68:703–710.
6. Wang D, Shao J, Rapacchi S, Middione MJ, Ennis DB, Hu P. Phase contrast MRI with flow compensation view sharing. Magn Reson Med 2015;73:505–513.
7. Srichai MB, Lim RP, Wong S, Lee VS. Cardiovascular applications of phase-contrast MRI. Am J Roentgenol 2009;192:662–675.
8. Vanninen RL, Manninen HI, Partanen PL, Vainio PA, Soimakallio S. Carotid artery stenosis: clinical efficacy of MR phase-contrast flow quantification as an adjunct to MR angiography. Radiology 1995;194: 459–467.
9. Bock J, Frydrychowicz A, Lorenz R, Hirtler D, Barker AJ, Johnson KM, Arnold R, Burkhardt H, Hennig J, Markl M. In vivo noninvasive 4D pressure difference mapping in the human aorta: phantom comparison and application in healthy volunteers and patients. Magn Reson Med 2011;66:1079–1088.
10. Thompson RB, McVeigh ER. High temporal resolution phase contrast MRI with multiecho acquisitions. Magn Reson Med 2002;47:499–512.
11. Gu T, Korosec FR, Block WF, Fain SB, Turk Q, Lum D, Zhou Y, Grist TM, Haughton V, Mistretta CA. PC VIPR: a high-speed 3D phase-contrast method for flow quantification and high-resolution angiography. Am J Neuroradiol 2005;26:743–749.
12. Negahdar M, Kadbi M, Tavakoli V, Heidenreich J, Amini AA. Comparison of Cartesian, UTE radial, and spiral phase-contrast MRI in measurement of blood flow in extracranial carotid arteries: normal subjects. SPIE Proc 2013;8672:86720A–86720A–9.
13. Griswold MA, Jakob PM, Heidemann RM, Nittka M, Jellus V, Wang J, Kiefer B, Haase A. Generalized autocalibrating partially parallel acquisitions (GRAPPA). Magn Reson Med 2002;47:1202–1210.
14. Pruessmann KP, Weiger M, Scheidegger MB, Boesiger P. SENSE: sensitivity encoding for fast MRI. Magn Reson Med 1999;42:952–962.
15. Kim D, Dyvorne HA, Otazo R, Feng L, Sodickson DK, Lee VS. Accelerated phase-contrast cine MRI using k-t SPARSE-SENSE. Magn Reson Med 2012;67:1054–1064.
16. Huang F, Akao J, Vijayakumar S, Duensing GR, Limkeman M. k-t GRAPPA: a k-space implementation for dynamic MRI with high reduction factor. Magn Reson Med 2005;54:1172–1184.
17. Madore B, Glover GH, Pelc NJ. Unaliasing by Fourier-encoding the overlaps using the temporal dimension (UNFOLD), applied to cardiac imaging and fMRI. Magn Reson Med 1999;42:813–828.
18. Jung B, Honal M, Ullmann P, Hennig J, Markl M. Highly k-t-space–accelerated phase-contrast MRI. Magn Reson Med 2008;60:1169–1177.
19. Lustig M, Donoho D, Pauly JM. Sparse MRI: the application of compressed sensing for rapid MR imaging. Magn Reson Med 2007;58: 1182–1195.
20. Tao Y, Rilling G, Davies M, Marshall I. Carotid blood flow measurement accelerated by compressed sensing: validation in healthy volunteers. Magn Reson Imaging 2013;31:1485–1491.
21. Kwak Y, Nam S, Akçakaya M, Basha TA, Goddu B, Manning WJ, Tarokh V, Nezafat R. Accelerated aortic flow assessment with compressed sensing with and without use of the sparsity of the complex difference image. Magn Reson Med 2013;70:851–858.
22. Middione MJ, Wu HH, Ennis DB. Convex gradient optimization for increased spatiotemporal resolution and improved accuracy in phase contrast MRI. Magn Reson Med 2014;72:1552–1564.
23. Hansen MS, Baltes C, Tsao J, Kozerke S, Pruessmann KP, Boesiger P, Pedersen EM. Accelerated dynamic Fourier velocity encoding by exploiting velocity-spatio-temporal correlations. Magn Reson Mater Phys Biol Med 2004;17:86–94.
24. Contur TE, Robinson BH. Analysis of encoding efficiency in MR imaging of velocity magnitude and direction. Magn Reson Med 1992; 25:233–247.
25. Breuer FA, Blaimer M, Heidemann RM, Mueller MF, Griswold MA, Jakob PM. Controlled aliasing in parallel imaging results in higher acceleration (CAIPIRINHA) for multi-slice imaging. Magn Reson Med 2005;53:684–691.